논문

FLAP DEFLECTION OPTIMZATION FOR TRANSONIC CRUISE PERFORMANCE IMPROVEMENT OF SUPERSONIC TRANSPORT WING

Hyoung-Jin Kim[*1], Shigeru Obayashi[*2], Kazuhiro Nakahashi[*2]

초음속 날개의 천음속 순항성능 향상을 위한 플랩 꺽임각 최적화

김 형진[*1], Shigeru Obayashi[*2], Kazuhiro Nakahashi[*2]

초음속 여객기의 천음속 순항 성능을 개선하기 위하여 날개의 플랩 꺽임각을 최적화하였다. 이를 위하여 3차원 Euler 코드와 adjoint 코드를 이용한 최적설계기법을 적용하였다. 설계변수로서, 앞전플랩 5개, 뒷전 플랩 5개 등 총 10개의 플랩의 꺽임각이 사용되었다. 설계과정중에 격자계 내부격자점의 수정을 위해 타원형방정식법을 이용하였다. 계산 시간의 단축을 위해 내부격자의 민감도는 무시하였다. 또한 본 설계문제에 근사구배기법의 적용가능성 여부를 조사하였다. 충격파가 없는 경우 앞전 플렙에 한하여 근사구배기법을 적용할 수 있음을 알았다. 최적설계기법으로 BFGS기법을 적용하여 항력을 최소화하였으며, 양력 및 날개 표면 마하수에 대한 제약조건을 적용하였다. 앞전 플랩의 최적화 및 앞전과 뒷전 플랩의 최적화 등 두 개의 설계 문제를 고려하였다. 성공적인 결과를 얻음으로써 본 설계방법의 타당성 및 효율성을 확인하였다.

Key Words: 초음속수송기(Supersonic transport), Adjoint method, 공력설계(aerodynamic design), 플랩 꺽임각 (flap deflection)

1. Introduction

Due to sonic boom restrictions, the next generation Supersonic Transport (SST) is required to cruise at a transonic speed over land, while cruising at a supersonic speed over water. In order to improve its transonic cruise performance, leading edge (LE) and trailing edge (TE) flaps have been considered as efficient tools that do not degrade supersonic cruise performance.[1,2] A SST wing cruising at a transonic speed is prone to flow separation because its leading edge usually has much smaller nose radius than those of transonic transport wings. Leading edge flaps can be very useful to avoid onset of flow separation in the transonic cruise regime.

Lovell[1] and Grenon[2] reported European research concerned with reducing drag at low speed and supersonic/transonic cruise conditions. In the references, LE flap optimization was adopted to improve transonic cruise performance and to avoid LE flow separation. Grenon[2] also reported the necessity of upward deflection of TE flaps in order to avoid flow separation near the wing tips.

In this study, we employed five LE flaps and five TE flaps to improve transonic

* 2001년 3월 12일 접수

*1 한국항공우주연구원 터보기계연구그룹

*2 Tohoku Univ. Sendai, Japan

performance of an experimental supersonic transport, which is under development by NAL (National Aerospace Laboratory) of Japan. The flap deflection angles are optimized using a gradient-based numerical optimization technique and a three-dimensional computational fluid dynamics (CFD) code.

With the advances in CFD and computing power of modern computers, aerodynamic design optimization methods utilizing CFD codes are more important than ever. Among several design optimization methods applicable to aerodynamic design problems, the gradient-based method has been used most widely due to its well-developed numerical algorithms and relatively small computational burden. In the application of gradient-based methods to practical aerodynamic design problems, one of the major concerns is the accurate and efficient calculation of sensitivity derivatives of an aerodynamic objective function. The finite difference approximation is the simplest way to calculate the sensitivity information since it does not require any sensitivity code. However, the accuracy of such an approach depends critically on the perturbation size of design variables and the flow initialization[3]. Recently, the complex variable method is drawing much attention as an accurate method for sensitivity calculation without any sensitivity analysis code, since the method does not show dependency on the step size of design parameters[4].

Sensitivity derivatives can be evaluated more robustly and efficiently by using a sensitivity analysis code based either on a direct method or an adjoint method. An adjoint method is preferable in aerodynamic designs because it is more economical when the number of design variables is larger than the total number of an objective function and constraints. Reuther et al[5], for example, designed aircraft configurations using a continuous adjoint method with Euler equations in a structured multi-block grid system.

For complex aerodynamic configurations, the unstructured grid approach has several advantages over the structured grid approach. This approach allows treatment of complex geometry with greater efficiency and less effort. It also has a greater flexibility in the adaptive grid refinement/unrefinement; thus the total number of grid points can be saved. Previous works on sensitivity analysis studies for unstructured grid approaches can be found in Ref.[5,6].

In this study, we adopt a discrete adjoint sensitivity code developed by Kim et.al[6] from a 3-D unstructured Euler solver based on a cell-vertex finite volume method. Sensitivity derivatives of an objective function are calculated efficiently and accurately by the adjoint code. Flap deflection angles are used as design variables. During the design process, interior grids are modified by the elliptic equation method. Grid sensitivities of the interior grids are neglected in order to reduce required computational time for the mesh sensitivity calculation.

The rest of this paper presents a brief review of the flow solver and the discrete adjoint code. Design methodologies are described including surface mesh deformation and interior mesh movement techniques. Design results utilizing the design method are finally given for the optimization of flap deflection angles of a SST wing. Design examples include LE flap deflection optimization and a simultaneous optimization of LE and TE flaps.

2. Flow Analysis

The Euler equations for compressible inviscid flows are written in an integral form as follows.

$$\frac{\partial}{\partial t}\int_{\Omega} \boldsymbol{Q} dV + \int_{\partial\Omega} \boldsymbol{F}(\boldsymbol{Q}) \cdot \boldsymbol{n}\, dS = 0 \quad (1)$$

where $\boldsymbol{Q}=[\rho, \rho u, \rho v, \rho w, e]^T$ is the vector of conservative variables; ρ the density; u, v, w the velocity components in the x, y, z directions; and e the total energy. The vector F(Q) represents the inviscid flux vector and n is the outward normal of $\partial\Omega$ which is the boundary of the control volume Ω. This system of equations is closed by the perfect gas equation of state with a constant ratio of specific heats.

The equations are solved by a finite volume cell-vertex scheme. The control volume is a non-overlapping dual cell. For a control volume, Eq.(1) can be written in an algebraic form as follows;

$$V_i \frac{\partial \mathbf{Q}_i}{\partial t} = -\sum_{j(i)} \Delta S_{ij} \mathbf{h}^{n+1}\left(\mathbf{Q}_{ij}^{+}, \mathbf{Q}_{ij}^{-}, \mathbf{n}_{ij}\right) \quad (2)$$

where ΔS_{ij} is a segment area of the control volume boundary associated with edge connecting points i and j. This segment area ΔS_{ij} as well as its unit normal $\mathbf{n}_{ij}$ can be computed by summing up the contribution from each tetrahedron sharing the edge. The term h is an inviscid numerical flux vector normal to the control volume boundary, and $Q_{ij}^{\pm}$ are flow variables on both sides of the control volume boundary. The subscript of summation, *j(i)*, means all node points connected to node i.

The numerical flux **h** is computed using an approximate Riemann solver of Harten-Lax-van Leer-Einfeldt-Wada(HLLEW)[7]. The second order spatial accuracy is realized by a linear reconstruction of the primitive gas dynamic variables $q=[\rho, u, v, w, p]^T$ inside the control volume using the following equation;

$$q(\boldsymbol{r}) = q_i + \psi_i \nabla q_i \cdot (\boldsymbol{r} - \boldsymbol{r}_i), \quad (0 \le \psi \le 1) \quad (3)$$

where **r** is a vector pointing to point (x,y,z), and i is the node index. The gradients associated with the control volume centroids are volume-averaged gradients computed by the surrounding grid cells. Venkatakrishnan's limiter[8] is used for the function ψ_i in Eq.(3) because of its superior convergence properties.

In order to integrate Eq. (2) in time, the Lower-Upper Symmetric Gauss-Seidel(LU-SGS) implicit method[9] is adopted.

3. Sensitivity Analysis

3.1 Direct Method

An aerodynamic sensitivity analysis begins with the fact that the discrete residual vector of the nonlinear flow equations is null for a converged flow field solution of steady problems, which can be written symbolically as

$$R_i[\boldsymbol{Q}, \boldsymbol{X}, \boldsymbol{B}] = 0, \quad (4)$$

where **X** is the grid position vector, $\boldsymbol{B}$ the vector of design variables. Equation (4) can be directly differentiated via the chain rule with respect to β to yield the following equation

$$\frac{dR_i}{d\beta} = \left[\frac{\partial R_i}{\partial Q}\right]\left\{\frac{dQ}{d\beta}\right\} + \{C_i\} = 0. \quad (5)$$

where $\{C_i\} = \left[\frac{\partial R_i}{\partial X}\right]\left\{\frac{dX}{d\beta}\right\} + \left\{\frac{\partial R_i}{\partial \beta}\right\} = 0.$

This equation is the direct sensitivity equation for the flow variable sensitivity $\{dQ/d\beta\}$. The vector $\{C_i\}$ has no relation with the $\{dQ/d\beta\}$, and thus, is constant throughout the solution process of the sensitivity equation for a design variable β. $\{dX/d\beta\}$ in the $\{C_i\}$ is a vector of grid sensitivity, which can be calculated by a finite-difference approximation or the direct differentiation of a routine for the

grid generation or modification. In order to find the solution $\{dQ/d\beta\}$ of Eq.(5) iteratively, a pseudo time term is added as follows to obtain the incremental form;

$$V_i\frac{\partial Q'}{\partial t}=\left[\frac{\partial R_i}{\partial Q}\right]\left\{\frac{dQ}{d\beta}\right\}^{n+1}+\{C_i\}, \qquad (6)$$

where $\mathbf{Q}'$ represents the solution vector $\{dQ/d\beta\}$. The above system of equations is solved with the LU-SGS scheme that is used for the flow solver. When the flow variable sensitivity vector is obtained, the total derivative of the objective function F can be calculated. The objective function F is usually an aerodynamic coefficient such as C_D, C_L, C_M, or differences of surface pressures with specified target pressures. F is a function of flow variables **Q**, grid position **X**, and design variables $\boldsymbol{B}$, i.e,

$$F=F(\boldsymbol{Q}(\boldsymbol{B}),\boldsymbol{X}(\boldsymbol{B}),\boldsymbol{B}). \qquad (7)$$

The sensitivity derivative of the cost function F with respect to a design variable β is given by

$$\left\{\frac{dF}{d\beta}\right\}=\left[\frac{\partial F}{\partial Q}\right]^T\left\{\frac{dQ}{d\beta}\right\}+\left[\frac{\partial F}{\partial X}\right]^T\left\{\frac{dX}{d\beta}\right\}+\left\{\frac{\partial F}{\partial \beta}\right\}, \qquad (8)$$

3.2 Adjoint Method

Since the total derivative of the flow equations in the steady state is null as can be seen in Eq.(5), we can introduce adjoint variables and combine Eqs. (5) and (8) to obtain

$$\left\{\frac{dF}{d\beta}\right\}=\left[\frac{\partial F}{\partial Q}\right]^T\left\{\frac{dQ}{d\beta}\right\}+\left[\frac{\partial F}{\partial X}\right]^T\left\{\frac{dX}{d\beta}\right\}+\left\{\frac{\partial F}{\partial \beta}\right\} + \{\lambda\}^T\left\{\left[\frac{\partial R}{\partial Q}\right]\left\{\frac{dQ}{d\beta}\right\}+\{C\}\right\} \qquad (9)$$

Coefficients of the flow variable sensitivity vector $\{dQ/d\beta\}$ form the following adjoint equation.

$$\left[\frac{\partial R}{\partial Q}\right]^T\{\lambda\}+\left\{\frac{\partial F}{\partial Q}\right\}=0, \qquad (10)$$

If one finds the adjoint variable vector $\{\lambda\}$ which satisfies the above adjoint equation, one can obtain the sensitivity derivative of F with respect to β without any information about the flow variable sensitivity vector $\{dQ/d\beta\}$. This makes the computational cost for the sensitivity analysis independent of the number of design variables. Equation (9) eventually becomes to the following form,

$$\left\{\frac{dF}{d\beta}\right\}=\left[\frac{\partial F}{\partial X}\right]^T\left\{\frac{dX}{d\beta}\right\}+\left\{\frac{\partial F}{\partial \beta}\right\}+\{\lambda\}^T\{C\} \qquad (11)$$

All the required differentiation for the sensitivity equations is conducted by hand-differentiation. More details on the sensitivity analysis such as boundary conditions and code validation can be found in Ref.[6]

4. Design Methodology

The present design method using the unstructured Euler solver and the adjoint method is applied to an unpowered experimental SST, which is under development by National Aerospace Laboratory of Japan as a basic study for the next generation supersonic transport.[12]

The objective of the present design study is defined as follows.

$$\text{Minimize } C_D \qquad (12)$$
$$\text{subject to } C_L = C_L^*$$

where C_D and C_L are drag and lift coefficients, respectively, and C_L^* is a specified target lift coefficient. If the lift constraint is dealt with as an explicit constraint in an optimizer, it requires an additional adjoint code computation for the C_L derivatives. In this study, therefore, the lift constraint is satisfied running the flow

solver in a fixed-lift mode, in which the incidence angle α is adjusted based on $C_{L\alpha}$ to obtain a lift coefficient satisfying the following inequality conditions:

$$C_L^* \leq C_L \leq 1.003\ C_L^* \quad (13)$$

Since we would like to minimize drag when $C_L = C_L^*$ at an adjusted incidence angle, the objective function $F = C_D$ should be modified as follows to consider the lift constraint consistently[6].

$$F = C_D - \frac{\left(\frac{\partial C_D}{\partial \alpha}\right)}{\left(\frac{\partial C_L}{\partial \alpha}\right)}(C_L - C_L^*) \quad (14)$$

4.1 Design Objective

The present design method using the unstructured Euler solver and the adjoint method is applied to an experimental SST wing with a flow-through type engine nacelle attached on its lower surface, which is under development by National Aerospace Laboratory of Japan as a basic study for the next generation supersonic transport.[9]

The objective of the present design study is defined as follows.

$$\text{Minimize } C_D \quad (13)$$
$$\text{subject to } C_L = C_L^*$$

where C_D and C_L are drag and lift coefficients, respectively, and C_L^* is specified. If the lift constraint is dealt as an explicit constraint in an optimizer, it requires an additional adjoint code computation for the C_L derivatives. In this study, therefore, the lift constraint is satisfied running the flow solver in a fixed-lift mode, in which the incidence angle α is adjusted based on $C_{L\alpha}$. Since we would like to minimize drag when $C_L = C_L^*$, i.e. at an adjusted incidence angle, the objective function $F = C_D$ should be modified as follows to consider the lift constraint consistently,

$$F = C_D - \frac{\left(\frac{\partial C_D}{\partial \alpha}\right)}{\left(\frac{\partial C_L}{\partial \alpha}\right)}(C_L - C_L^*) \quad (14)$$

where CL is a lift coefficient without any incidence angle variation. The second term on the RHS of Eq.(14) acts as a penalty term, which prevents the design from reducing the drag by simply reducing the lift. The same expression for the modified objective function was suggested in a variational form by Reuther et al.[5].

An additional constraint for the suppression of boundary layer separation is required, since the present design study is based on inviscid flow physics only. It is implemented by imposing upper bounds of effective Mach numbers on the wing surface as was employed in Refs.[1,2]. The effective Mach number is calculated from actual local Mach number considering local sweep angle which varies gradually from the leading edge sweep angle to trailing edge sweep angle. The upper bound of the effective Mach number is 1.3 for the first half chord, 1.1 for the second half chord region. This constraint is treated as a penalty term added explicitly to the Eq.(14) as follows:

$$F_{new} = F + w \sum_{surface} \max(0, p_{\lim} - p_{surf}) \Delta S \quad (15)$$

where w is a weighting factor multiplied to the penalty term, p_{lim} is pressure limit calculated from the Mach number limit by the isentropic relation, and ΔS is an area of a surface grid cell.

4.2 Design Parameters and Grid Modification Method

In the present design study, design variables are deflection angles of ten flaps: five LE and five TE flaps. Figure 1 shows definitions of LE and TE flaps on the main wing of the experimental SST. Chordwise length of all the LE flaps is set to be 40 percent of the wing

tip chord length, and TE flap length is defined to be 20 percent chord of TE kink location inboard and 20 percent chord of local sections outboard. Flap deflections are made such that each grid point on the flaps is translated along the z axis only according to its distance from the hinge line, and thus, wing planform is kept the same as the initial geometry. All flap angles are defined on a plane normal to the hinge line. Counterclockwise flap deflections are defined to be positive; i.e. downward deflections for LE flaps and upward deflections for TE flaps are positive.

Between every two flaps, wing surface geometry is linearly interpolated instead of being split. The thickness and camber of the wing section geometry is kept the same as the initial geometry so that supersonic cruise performance of the aircraft is not penalized by the flap design for transonic cruise.

When the surface grid is modified, the interior grid points should be moved accordingly. In the structured grid approach, the interior grid positions can be moved with relative ease using an algebraic mesh movement strategy which modifies the grid point coordinates along a grid line of the same index. In the unstructured grid method, however, such a simple grid modification method cannot be applied, and a more sophisticated grid movement method is needed.

For the movement of the grid points with the perturbed surface grid, we used the elliptic partial differential equation method proposed by Crumpton and Giles[13]. In the method, the displacement $\mathbf{dx}$ from initial grid point $\boldsymbol{x0}$ is prescribed by the following equation with Dirichlet boundary conditions

$$\nabla \cdot (k \nabla \delta x) = 0. \tag{16}$$

Diffusion coefficient k is constant in each cell and is given by

$$k = \frac{1}{\max(Vol, \varepsilon)}, \tag{17}$$

where Vol is the control volume of each grid point and ε is a small positive number to prevent k from becoming negative. The elliptic equation (16) is discretized by a finite volume method, and subsequent linear algebraic equations are solved by the conjugate gradient method[14]. Required computational time to obtain converged solution δx was same as that of a few iterations of the Euler solver.

4.3 Grid Sensitivity

The elliptic equation method for the interior grid movement is differentiated for the grid sensitivity calculation for the vector {C} in Eq.(9) with respect to each geometric design variable. Since this requires almost the same computational cost as with the grid movement procedure, the total computational burden would be a substantial amount if the number of design variables becomes large.

One possible way to reduce the computational burden of the grid sensitivity calculation is to neglect the grid sensitivity of interior node points. It has been shown in Ref[6,15] that in cases with inviscid flows interior grid sensitivity can be ignored for design variables not associated with a translation of a body. In this study, therefore, only the surface grid sensitivities are considered, and interior grid sensitivities for the flap deflection are ignored for efficiency.

4.4 Approximate Gradient Evaluation

Mohammadi[16] suggested the following approximate gradient evaluation which neglects the sensitivity of an objective function with respect to flow variables when the objective function is based on a boundary integral;

$$\left\{\frac{dF}{d\beta}\right\} = \left[\frac{\partial F}{\partial Q}\right]^T \left\{\frac{dQ}{d\beta}\right\} + \left[\frac{\partial F}{\partial X}\right]^T \left\{\frac{dX}{d\beta}\right\}$$

$$\cong \left[\frac{\partial F}{\partial X}\right]^T \left\{\frac{dX}{d\beta}\right\} \tag{18}$$

This approximation is based on an observation that the dominant part in the gradient is the partial derivative with respect to

geometry and not to the flow variable when a small change in geometry causes very slight variations in flow variables. This would, of course, not be applicable to general cases, and, therefore should be adopted with great care. However, if it is found to be valid for the problem at hand, computational cost for the sensitivity analysis can be drastically reduced since any analysis of sensitivity equations is not required and only the partial differentiation of the objective function with respect to geometry change is needed.

4.5 Optimization Method

For the unconstrained minimization of the objective function in Eq.(20), the ADS(Automated Design Synthesis) program[17] was used as an optimizer. The BFGS(Broydon-Fletcher-Goldfarb-Shanno) method[18] is adopted in order to determine a search direction. One-dimensional search is then conducted using a quadratic polynomial interpolation. Detailed algorithms and methodologies of the optimization method are described in Ref.18.

5. Design Results

Design conditions are a free-stream Mach number of 0.95 and C_L of 0.2. Figure 2 shows the SST configuration and surface grids of initial geometry. The number of nodes and cell for the adopted volume grid are about 270,000 and 1,500,000, respectively.

Before we go on to the design optimization results, accuracy comparisons of sensitivity gradients are made for the simplification ignoring interior grid sensitivity and the approximate gradient evaluation using geometric sensitivity only. Figure 3 shows sensitivity derivatives of the objective function with respect to the ten flap deflection angles for initial geometry without any flap deflection. Derivatives obtained without interior grid sensitivity show good agreement with those calculated with surface grid sensitivity only. Similar results were also reported in a previous work by the authors[6] for supersonic flow conditions.

In Fig.3, sensitivity derivatives obtained by the approximate gradient evaluation method are also presented(diamond symbols). It is interesting to note that the derivatives with respect to the LE flap deflection calculated by the AGE show similar trends to those obtained by the adjoint method, while those with respect to the TE flap have opposite signs with similar magnitude. This implies that deflection of LE flaps causes little change in flow variables, and therefore the effect of geometry change dominates in the total sensitivity derivatives for the present flow condition. On the other hand, for the TE flaps, the variation of the flow variables due to the flap deflection dominates in the total derivatives of the objective function. In order to compare the direction of the sensitivity derivative vector for LE flaps, normalized vector components are compared in Fig.4, which shows that the direction of the two vectors agrees well each other, although their magnitudes have some variations. This may allow us to get successful results of LE flap optimization with the sensitivity information obtained by the approximate gradient evaluation method.

In this study, two design problems are considered; one involves a LE flap design, and the other involves simultaneous design of LE and TE flaps. We compared LE flap design results by the approximate gradient evaluation and by the adjoint method. For the LE and TE flap design, the adjoint method is used since the AGE does not give reliable sensitivity information for the TE flaps.

The density residual of the Euler solver was reduced by four orders from the initial value, and that of the adjoint code by two orders. Lower and upper bounds of the ten design variables are set as -30 and +30 degrees, respectively, so that the design space is large

enough and the design process is not disturbed by the bounds.

5.1 Design I: LE flap design

We conducted the LE flap design optimization by the AGE and by the adjoint method with five flap deflection angles as design variables. Although the approximate gradient evaluation gives accurate search direction for the initial geometry, the deviation of the normalized gradient vector components from the adjoint result increased to 15 ~ 30 % as the design process continued to the second iteration as can be seen in Fig. 5. This is because a shock wave was about to form on the upper surface, and the flow variable change due to the LE flap deflection would increase drastically if a shock wave were to form on the wing surface.

Table 1 presents LE flap design results by the two sensitivity calculation methods. For both cases, little improvement was achieved after the second design iteration, and the drag coefficient was reduced by about 12 counts retaining the lift coefficient as the specified value. Because of the increased inaccuracy of the AGE, no perceivable flap deflection changes were made after the first iteration, whereas the adjoint method provided accurate search direction so that flaps are deflected a few degrees more, and slight performance improvement was made accordingly. However, in spite of the inaccurate (but of right sign) sensitivity information of the AGE after the second iteration, the difference of resulted drag coefficients was only about 0.2 count. This is because a local minimum solution was found by the first design iteration, and after that, accuracy of the sensitivity derivatives seems not to affect the final results.

Comparing the results by the two methods shown in Table 1, one notes that LE flaps located inboard (flap #1, 2, and 3) show similar deflection angles and the same is true for those located outboard (flap #4, 5). This implies that one may employ two flaps only; one for the inboard and the other for the outboard for a practical design of LE flap deflection for SST without major loss in aerodynamic performance.

Table 1. Results of design I; LE flap design

		initial	Method of sensitivity derivative calculation	
			Appr. gradient Evaluation (Δ%)	Adjoint method(Δ %)
C_L		0.2002	0.2002 (0.0)	0.2000 (-0.1)
C_D		0.008087	0.006922 (-14.41)	0.006901 (-14.67)
L/D		24.76	28.93 (+16.84)	28.98 (+17.04)
Flap angles (deg.)	δ_1	0	4.63	6.18
	δ_2	0	5.01	6.75
	δ_3	0	4.40	5.76
	δ_4	0	17.27	19.27
	δ_5	0	17.10	19.99

Figure 6(a) shows surface pressure distributions at five wing sections that lie at the centerline of each LE flap. Leading edge suction peaks have been reduced by the flap deflection, and the minimum pressure point occurs on the hinge line of the flaps. It is noted that the surface Mach number limits are not touched by the initial and design pressure distributions. The surface Mach number limitation was the main factor that kept the LE flap angles from being increased more in Ref.[1,2]. In the present example, however, it did not act as an active constraint, and thus, the penalty term in Eq.(20) was always zero during the design process. This is because of the fact that the SST wing adopted as an initial geometry of this study was designed using a Natural Laminar Flow (NFL) concept

for the supersonic cruise condition, which made the leading edge of the wing very blunt[12]. The surface pressure contours on the wing upper surface are depicted in Fig.6(b). It is clear from this figure that the location of minimum pressure moved from leading edge to flap hinge line.

5.2 Design II : design of LE and TE flaps

In the present design example, we tried to optimize the LE and TE flap angles with the design I obtained by using the AGE method as the initial point. The sensitivity analysis showed that all the TE flaps would be deflected downward to minimize the objective function. This is an interesting point reminding us of the necessity of upward deflection of TE flaps that was reported in Ref.2 in order to avoid flow separation near the wing tips. We can expect that the direction and magnitude of TE flap deflection would be influenced by the performance improvement and by suppression of flow separation.

At the first optimization iteration, it was found that the maximum Mach number limit is a main factor that limits the deflection of inboard TE flaps, i.e. flap #6, 7, and 8. As a result, the downward deflection angles for the first iteration were only about 0.5 degrees inboard and about 0.3 outboard, and the drag coefficient was reduced by about one-and-half counts. Figure 6(c) shows inboard section pressure distributions obtained by the one-dimensional search of the first iteration. Outboard pressure distributions do not differ much from those of design example I depicted in Fig.6(a) and, therefore, are not presented here. The inboard flow is reaccelerated near the hinge of the TE flaps, and a shock appears just before the TE to recover the stagnation pressure. Although the solution did not violate the maximum Mach limit, it was still believed that it would promote flow separation in the real viscous flow, due to the shock wave being too close to the TE. This was the case for a design with the undeflected wing shape as an initial point. This shows the difficulty of imposing the maximum Mach number limit on the wing surface. More sophisticated definition of Mach limits are required so that this kind of aerodynamic optimization problems can be attacked by using Euler codes rather than by more expensive Navier-Stokes computations.

Since the near-TE shock wave occurred for downward TE flap deflection of about 0.5 degree only, we decided to freeze (i.e. not to deflect) the inboard TE flaps (flaps #6,7 and 8) and to design outboard flap deflections (flaps #9 and 10) only in addition to LE flaps. This design example was terminated after five iterations since there was no further performance improvement. Table 2 presents the LE and TE flap design results with inboard TE flaps frozen. Additional drag reduction of about two counts was made by the present design study from the optimized LE flaps of design I. Figure 8 shows surface pressure distributions of the design. Pressure distributions of inboard sections show little difference from those of initial geometry except the fact that upper surface pressures have been slightly increased. This is because the downward deflection of TE flaps increased the lift, and therefore, the incidence angle was decreased to match the specified target lift coefficient. Outboard wing sections show the effects of TE flaps deflection; the flow is accelerated around the TE flap hinge line, and section lift is increased.

It should be noted that the outboard TE flaps can be deflected by about two degrees without any shock waves, whereas the inboard LE flaps suffer from strong shock wave formation and flow separation with a deflection of merely 0.5 degree. This is because the TE sweep angle of the experimental SST of NAL is 30 degrees outboard, while there is no TE sweep

inboard. This sweep effect allows the outboard flow to have a higher separation margin than the inboard flow since the former has much lower effective Mach numbers on the wing surface near the TE than the latter.

Table 2. Results of design II; LE flap design

			Initial	Design
C_L			0.2002	0.1999(-0.15)
C_D			0.006922	0.006723(-2.3)
L/D			28.93	29.66(+2.5)
Flap angles (deg.)	LE (downward +)	δ_1	4.63	5.17
		δ_2	5.01	5.60
		δ_3	4.40	4.88
		δ_4	17.27	18.00
		δ_5	17.10	18.06
	TE (upward +)	δ_6	0	0
		δ_7	0	0
		δ_8	0	0
		δ_9	0	-2.26
		δ_{10}	0	-1.68

6. Concluding Remarks

Leading edge/trailing edge flaps deflections are optimized to improve transonic cruise performance of a supersonic transport aircraft without degrading its supersonic performance. An aerodynamic design optimization system combining an optimization package, an unstructured Euler solver, and the discrete adjoint method was employed for efficient design studies. Deflection angles of five leading edge flaps and five trailing edge flaps are defined as design variables. The approximate gradient evaluation method, which ignores the effect of flow variable change due to the geometry perturbation on sensitivity derivatives, was found to be applicable to the design of leading edge flap angles; however, the AGE method gives totally wrong sensitivity information for the trailing edge deflections. By the design of leading edge flaps only, drag was reduced by about 12 counts and the lift-to-drag ratio was increased by 17 percent. With this result as an initial point, a simultaneous design of leading edge/trailing edge flaps was conducted to obtain additional two-count reduction of drag coefficient. Inboard trailing edge flaps were frozen in order to avoid flow separation on the flaps. Deflection of outboard trailing edge flaps had much less effect on flow separation than the inboard flaps because of the sweep back of outboard trailing edge.

References

[1] Lovell, D. A., European Research to Reduce Drag for Supersonic Transport Aircraft, AIAA99-3100, June 1999.

[2] Grenon, R., Numerical Optimization in Aerodynamic Design with Application to a Supersonic Transport Aircraft, NAL International Workshop on Supersonic Transport Design, March 1998, Tokyo, Japan.

[3] Eyi, S. and Lee, K. D., Effect of Sensitivity Calculation on Navier-Stokes Design Optimization, AIAA 94-0060, Jan. 1994.

[4] Anderson, W. K., Whitfield, D. L., Newman III, J. C., and Nielson, E. J., Sensitivity Analysis for the Navier-Stokes Equations on Unstructured Meshes, AIAA 99-3294, June, 1999.

[5] Reuther, J. J., Jameson, A., Alonso, J. J., Rimlinger, M. J., and Saunders, D., Constrained Multipoint Aerodynamic Shape

Optimization Using an Adjoint Formulation and Parallel Computers, Part 1, J. of Aircraft, vol. 36, No.1, pp51-60, 1999.

[6] Kim, H. J., Sasaki, D., Obayashi, S., and Nakahashi, K., Aerodynamic Optimization of Supersonic Transport Wing Using Unstructured Adjoint Method, accepted for publication in AIAA J., 2001.

[7] Obayashi, S., and Guruswamy, G. P., Convergence Acceleration of an Aeroelastic Navier-Stokes Solver , AIAA J. Vol.33, No.6, pp. 1134-1141, 1995.

[8] Venkatakrishnan, V., On the Accuracy of Limiters and Convergence to Steady State Solutions, AIAA Paper 93-0880, January 1993.

[9] Yoon, S. and Jameson, A., Lower-Upper Symmetric-Gauss-Seidal Method for the Euler and Navier-Stokes Equations, AIAA J., Vol.26, No.9 pp. 1025-1026, 1988.

[10] Jameson, A., and Turkel, E., Implicit Schemes and LU Decompositions, Mathematics of Computation, Vol.37, No.156, pp. 385-397, 1981.

[11] Sharov, D., and Nakahashi, K., Reordering of Hybrid Unstructured Grids for Lower-Upper Symmetric Gauss-Seidel Computations, AIAA J., Vol.36, No.3, pp. 484-486, 1998.

[12] Iwamiya, T., NAL SST Project and Aerodynamic Design of Experimental Aircraft, Proc. Computational Fluid Dynamics 98, Vol.2, ECCOMAS 98, John Wiley & Sons, Ltd. pp. 580-585, 1998.

[13] Crumpton, P. I. and Giles, M. B. Implicit Time Accurate Solutions on Unstructured Dynamic Grids, AIAA 95-1671, June, 1995.

[14] Press, W. H., Teukolsky, S. A., Vetterling, W. T., and Flannery, B. P., Numerical Recipes in Fortran, 2nd ed. Cambridge Univ. Press, Cambridge, England, UK, 1992.

[15] Anderon, W. K., and Venkatakrishnan, V., Aerodynamic Design Optimization on Unstructured Grids with a Continuous Adjoint Formulation, AIAA 97-0643, Jan. 1997.

[16] Mohammadi, B., Flow Control and Shape Optimization in Aeroelastic Configurations, AIAA 99-0182, Jan.1999.

[17] Vanderplaats, G. N., ADS A Fortran Program For Automated Design Synthesis version 3.00, Engineering Design Optimization, INC., 1987.

[18] Vanderplaats, G. N., Numerical Optimization Techniques for Engineering Design: With Applications, McGraw Hill, N.Y., 1984.

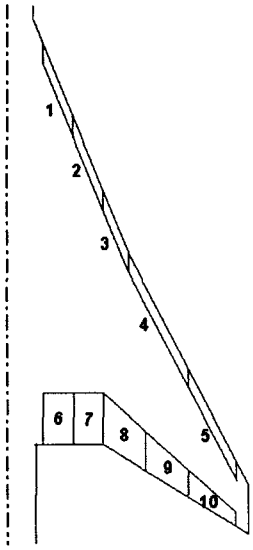

Fig. 1 Definition of leading edge and trailing edge flaps

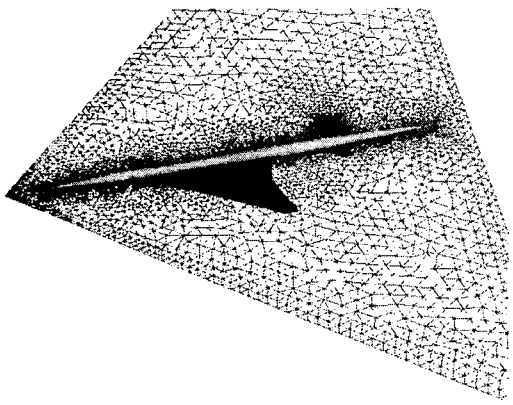

Fig. 2 Surface geometry of NAL experimental SST configuration and grids on symmet ric plane

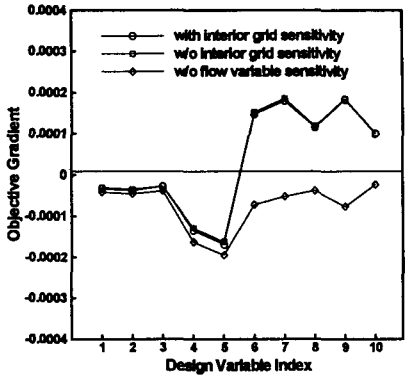

Fig. 3 Comparison of sensitivity derivatives for initial geometry

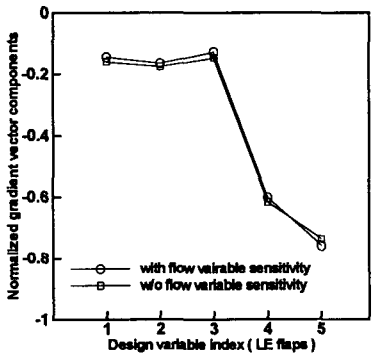

Fig. 4 Comparison of normalized sensitivity derivatives: At initial geometry

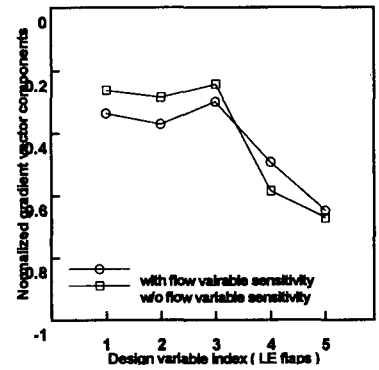

Fig. 5 Comparison of normalized sensitivity derivatives: After design iteration two

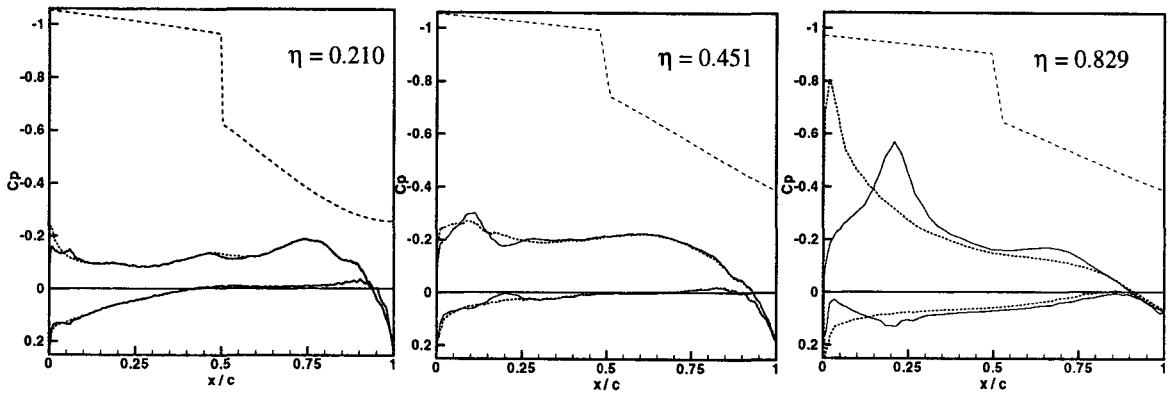

(a) LE design results by AGE (design I)

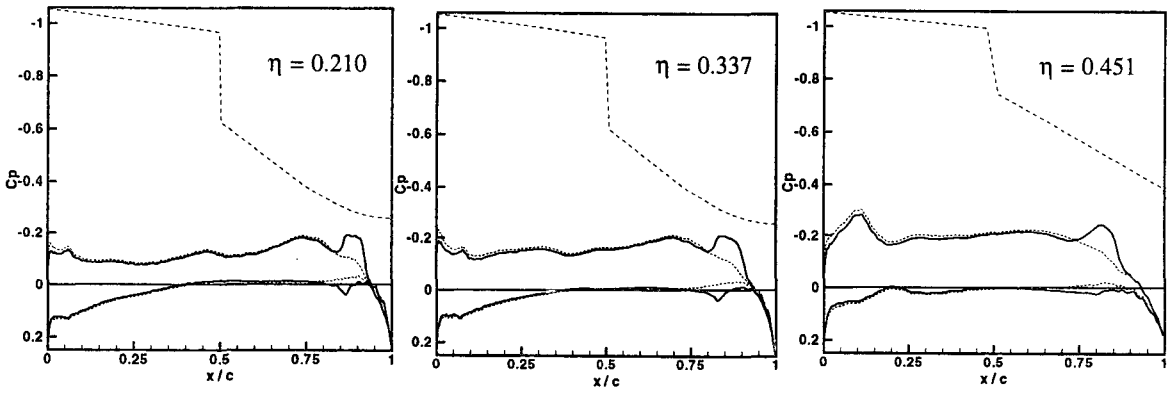

(b) LE & TE design results with inboard flap deflection activated

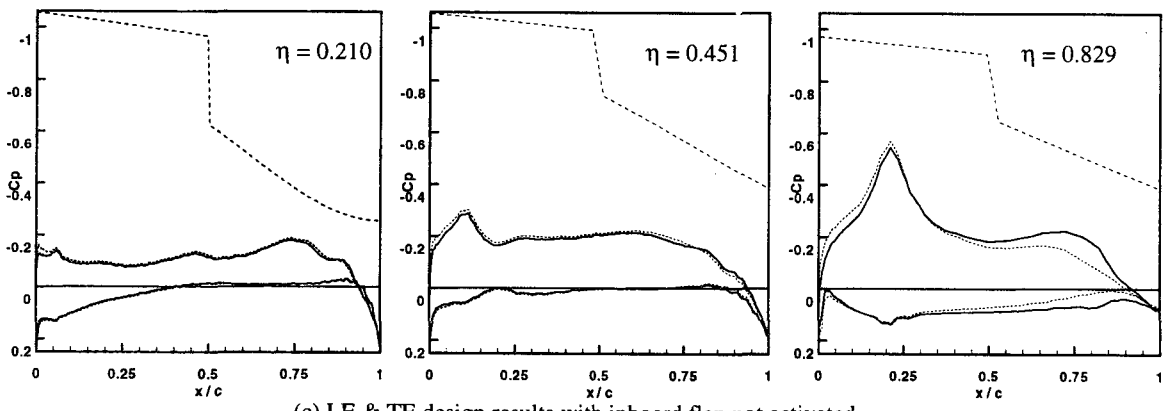

(c) LE & TE design results with inboard flap not activated

Fig.7 Design results : surface pressure distributions